Indexing of satellite images with different resolutions by wavelet features

Bin Luo, Jean-François Aujol, Yann Gousseau, Saïd Ladjal

***Abstract*— Space agencies are rapidly building up massive image databases. A particularity of these databases is that they are made of images with different but known resolutions. In this paper, we introduce a new scheme allowing to compare and index images with different resolutions. This scheme relies on a simplified acquisition model of satellite images and uses continuous wavelet decompositions. We establish a correspondence between scales which permits to compare wavelet decompositions of images having different resolutions. We validate the approach through several matching and classification experiments, and we show that taking the acquisition process into account yields better results than just using scaling properties of wavelet features.**

I. INTRODUCTION

Over the last years, space agencies have built up massive image databases. For example, the CNES (the French space agency) gets each day several terabytes of data from its satellites. These institutions need efficient tools to index and search their image databases. One particularity of satellite image databases, compared to e.g. natural image databases, is that they are constituted by images with different but known resolutions[1] depending on the satellite which acquires them. In contrast, the relationship between the size of objects and pixels is usually unknown for natural images. Moreover, this relationship depends on the position of objects in the scene, so that the notion of resolution itself has little general meaning for natural images. This obvious fact made it necessary to develop scale invariant local features for many computer vision tasks, see e.g. [1]. For the indexing of texture, it makes sense to assume a uniform resolution through the image. Since this resolution is usually unknown, many scale invariant indexing schemes have been developed, see e.g. [2], [3], [4], and [5] for a review. Our purpose in this paper is quite different. First, the resolution of satellite images is usually a known parameter, at least if we neglect tilts of the optical device and if we assume that the scene being captured is approximately flat. Therefore, our goal is to be able to compare two images knowing their resolution difference. Second, a resolution change is more complicated than just a scale change, since it usually involves an optical device and an imaging captor. In a previous work, [6], [7], this process was modeled as a convolution followed by a sampling and its effect on the computation of a characteristic scale was studied. In this paper, we make use of the same model and propose a scheme to compare features extracted from images at different resolutions. Observe that several works have been performed to extract image features that are invariant with respect to resolution changes [8], [9]. Again, our purpose is quite different since we wish to be able to compare images with different but *known* resolution.

Many features have been proposed to index satellite images [10], [11], [12], [13], [14]. In this work, we only consider mono-spectral images and classically choose to index them using texture features. In particular, wavelet features have been proved suitable for texture indexing or classification [15], [16], [17], [18], [19], [20], [21], [22]. Wavelet features have already been used for indexing remote-sensing images in [23]. The aim of the proposed approach is to investigate the interplay between resolution and wavelet features and to propose a scheme for the comparison of images with different resolutions. Preliminary results of the present work were presented in [24].

The plan of the paper is the following. In Section II a simplified model for the acquisition of satellite images is introduced. In Section III, we recall how the marginals of wavelet coefficients can be used for the indexing of images. In Section IV, a method is given to compare features extracted at different resolutions. In Section V, the dependence of features upon resolution is checked using satellite images from the CNES and the proposed scheme is validated through classification experiments. We then conclude in Section VI.

II. MODEL OF THE ACQUISITION PROCESS

A digital image f_r at resolution r is obtained from a continuous function f (representing the scene under study) through an optical device and a digital captor. Neglecting contrast changes and quantization, the effect of the imaging device can be modeled as follows,

$$f_r = \Pi_{S_r}(G * f) + n,$$

where G is the convolution kernel, $S_r \subset \mathbb{Z}^2$ the sampling grid at resolution r, Π_{S_r} the Dirac comb on S_r and n the noise. In what follows, we will take interest in the effect of the acquisition model on the wavelet coefficients of f_r. Therefore, and assuming that we will neglect coefficients at the smallest scales, we will assume that $n = 0$. Moreover, we will assume that $S_r = r\mathbb{Z}^2$, that is a regular and square sampling grid with step r. We thus neglect the satellite vibrations and scan acquisition. Last and more importantly, according to [25], [26], the response of an ideal optic aperture can be accurately approximated by a Gaussian kernel. We will therefore assume

B. Luo is with TELECOM ParisTech, CNRS UMR 5141, CNES-DLR-ENST Competence Centre, Paris, France.

Y. Gousseau and S. Ladjal are with TELECOM ParisTech, CNRS UMR 5141, Paris, France.

J-F. Aujol is with CMLA, ENS Cachan, CNRS, UniverSud, Cachan, France.

[1] By resolution, we mean the true pixel size in meter.

that G is an isotropic Gaussian kernel, thus neglecting the specificity of the satellite optics, the real response of the captor and motion blur. This is probably the strongest assumption made in this paper. The motivation behind it is mainly the tractability of forecoming computations, as will become clear soon. Last, we assume that the standard deviation of the kernel is proportional to the resolution. In the experimental section, we will check that these assumptions are not too restrictive by considering real satellite images. To summarize, we assume the following acquisition model :

$$f_r = \Pi_r(f * k_{rp}), \tag{1}$$

where

$$k_{rp}(x,y) = \frac{1}{2\pi r^2 p^2} \exp\left(-\frac{x^2+y^2}{2r^2p^2}\right), \tag{2}$$

Π_r is the Dirac comb on $r\mathbb{Z}^2$, that is,

$$\Pi_r = \sum_{i,j\in\mathbb{Z}} \delta_{(ir,jr)},$$

and the parameter p is a characteristic of the acquisition process, which characterizes the width of the convolution kernel: the larger the value of p, the more blurred the image.

III. Wavelet features for texture indexation

Based on empirical observations, S. Mallat [27] proposed to model the marginals of wavelet coefficients of natural images by Generalized Gaussian Distributions (*GGD*). That is, writing $h(w)$ for the density of the distribution of coefficients w at some scale and orientation,

$$h(w) = Ke^{-(|w|/\alpha)^\beta}. \tag{3}$$

It is shown in [15], [16], [17] that the parameters α and β of GGD can be used as efficient features for texture indexing and classification. It is possible to compute these parameters from the estimation of the first and second order moments of $|w|$ [27]: we denote them respectively by $m_1 = \int |w|h(w)dw$ and $m_2 = \int w^2 h(w)dw$. More precisely, $m_1 = \alpha\Gamma(2/\beta)\Gamma(1/\beta)^{-1}$ and $m_2 = \alpha^2\Gamma(3/\beta)\Gamma(1/\beta)^{-1}$, where Γ stands for the Gamma function.

In this paper, for simplicity, we address the problem of relating features m_1 and m_2 to resolution changes. Adapting the results to α and β is then straightforward and this can be useful when using the Kullback-Leibler distance in a classification task, see [16].

In order not to be restricted to dyadic resolution changes, continuous wavelet transform [28] is used instead of the more classical discrete wavelet transform. Moreover, *we consider mother wavelets obtained as derivatives of a Gaussian kernel* in horizontal, vertical and diagonal directions. This important assumption is motivated by the simplified model for resolution changes presented in the previous section, as will be shown by the computations of Section IV-A.

Figure 1 shows a histogram of absolute values of wavelet coefficients, illustrating the soundness of the use of GGDs to model such distributions.

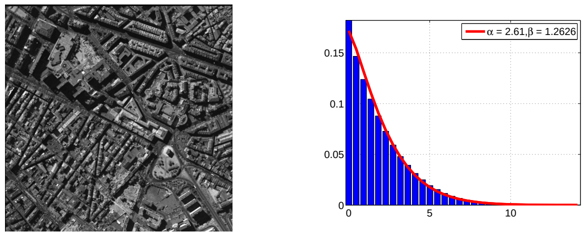

(a) Marseille (b) Histogram

Fig. 1. (a) Image of Marseille at resolution $0.707m$ (©CNES); (b) Histogram (blue bars) of wavelet coefficients of image (a) at scale 5 (horizontal) and the approximation by GGD (red curve).

IV. Wavelet features and resolution changes

A. Resolution Invariance

a) Notations: The discrete version of the Gaussian kernel with standard deviation t (t being given in pixels) is denoted by $\tilde{k}_t$. Let us define the discrete wavelet coefficients as (recall that the wavelets we use are derivatives of the Gaussian kernel)

$$w_{q,r,t} = \Delta_q \tilde{k}_t \tilde{*} f_r = \tilde{k}_t \tilde{*} \Delta_q f_r \tag{4}$$

where $q \in \{0,1,2,3\}$, Δ_q stands for the difference between adjacent pixels in the horizontal ($q=0$), vertical ($q=1$) or diagonal ($q=2,3$) direction, $\tilde{*}$ stands for the discrete convolution operation.

b) Resolution invariance: Recall that the image f_r at resolution r is obtained as $f_r = \Pi_r(k_{rp} * f)$. From Equation (4), we therefore have

$$\begin{aligned} w_{q,r,t} &= \tilde{k}_t \tilde{*} \Delta_q \Pi_r(k_{rp} * f) \\ &\approx \tilde{k}_t \tilde{*} \Pi_r(r\partial_q(k_{rp} * f)), \end{aligned} \tag{5}$$

where ∂_q is the continuous directional derivative at orientation q. This last approximation is detailed in the Appendix.

Next, we assume that the inversion between the convolution and the sub-sampling is appropriate for non-aliased images such as $k_{rp} * f$ when p is at least, say, $1/2$. The validity of this assumption on real images has been checked in [7]. Assuming that $\tilde{k}_t \approx k_{rt}$ (see [7]), and that the continuous and discrete convolutions are equivalent, we have

$$w_{q,r,t} \approx r\Pi_r(k_{rt} * k_{rp} * \partial_q f). \tag{6}$$

Using the semi-group property of the Gaussian kernel, it can be deduced that

$$\frac{w_{q,r,t}}{r} \approx \Pi_r(k_{r\sqrt{t^2+p^2}} * \partial_q f). \tag{7}$$

The accuracy of this approximation will be computed in the appendix.

Assume now that we have two images f_{r_1} and f_{r_2} of the same scene at resolutions r_1 and r_2. From (7), we deduce that if we choose scales t_1 and t_2 such that

$$r_1\sqrt{t_1^2+p^2} = r_2\sqrt{t_2^2+p^2}, \tag{8}$$

then

$$m_1(q,r_1,t_1)/r_1 \approx m_1(q,r_2,t_2)/r_2 \tag{9}$$

$$m_2(q,r_1,t_1)/r_1^2 \approx m_2(q,r_2,t_2)/r_2^2 \tag{10}$$

with

$$m_1(q,r,t) = \frac{1}{n_r}\sum |w_{q,r,t}|,$$

$$m_2(q,r,t) = \frac{1}{n_r}\sum |w_{q,r,t}|^2,$$

where n_r is the size of the discrete image f_r and the sum is taken over the image domain (notice that, since we use a continuous wavelet transform, w has the same size as f_r). These equalities (Formula (9) and (10)) permit to compare wavelet features from f_1 and f_2. In what follows, we denote by $\Theta_{q,r,t} = \{m_1(q,r,t), m_2(q,r,t)\}$ the wavelet features at scale t and direction q extracted from f_r.

c) Remark about the naive choice $p = 0.0$: A naive assumption could be made that for the same scene f, if we keep

$$r \times t = C \tag{11}$$

where C is a constant, the parameter set is also constant (after the correct normalization). However, this assumption is not sufficient because it approximates the resolution change by a simple zoom, which is not consistent with the acquisition process modeled in Section II. We will see in Section V that such a naive choice leads to poor numerical results compared with the use of Equation (8). In what follows, we will call "naive choice" the use of $p = 0$ in Equation (8).

d) Tuning of p: To use Equation (8), one needs to know the value of p. This is a characteristic of the acquisition process (see Equation (1)). This can therefore be tabulated once for each satellite. Observe that if one considers two images f_{r_1} and f_{r_2} with different resolutions, it is very likely that they originate from different satellites and that the corresponding values of p be different. In this case, writing p_i for the value of p corresponding to resolution r_i ($i = 1, 2$) it is straightforward to show that Equation (8) can be generalized to

$$r_1\sqrt{t_1^2 + p_1^2} = r_2\sqrt{t_2^2 + p_2^2}. \tag{12}$$

This equality again ensures that approximations (9) and (10) hold and permits the comparison of wavelet features from f_{r_1} and f_{r_2}. In what follows, for the sake of simplicity, we will assume that $p_1 = p_2$ and therefore use Equation (8).

B. Wavelet features and resolution

As explained in the introduction, the aim of this paper is to propose a way to compare the features originating from two images with different and known resolutions. One way to achieve this is to modify the features (i.e. the first and second order moments m_1 and m_2) extracted at resolution r_1 to compare them with the features extracted at resolution r_2. Assume that we have f_{r_1} the image at resolution r_1 of a given scene, and that we want to predict its features at resolution r_2. From Equations (7)–(10), we deduce the following scheme:

- Compute the wavelet coefficients for f_{r_1} at scales t_i, $i = 1, 2, 3, \ldots, N$;
- Estimate the parameters Θ_{q,r_1,t_i} from the wavelet coefficients at scales t_i for resolution r_1 ;
- For resolution r_2, compute the scales t'_i corresponding to t_i according to (see Equation (8))

$$t'_i = \sqrt{\frac{r_1^2}{r_2^2}(t_i^2 + p^2) - p^2} \tag{13}$$

- Define $\tilde{\Theta}_{q,r_2,t'_i} = \Theta_{q,r_1,t_i}$ at scales t'_i.

By using such an algorithm, it is now possible to compare images taken at different resolutions and, for instance, to train classification methods on a set of images at only one resolution and to apply the recognition criteria to images at different resolutions.

V. Experiments and results

A. Image database

In the following sections, we experimentally validate the proposed scheme for comparing wavelet features. These experiments are carried on an image database provided by the CNES (the French space agency). This database is made of various scenes (such as fields, forests and cities). Each scene has been acquired as an aerial image at resolution $0.25m$. Then, for each scene, the CNES has simulated images at various resolutions, using realistic satellite modeling. The available resolutions range from $0.5m$ to $4m$, according to a geometric progression with ratio $2^{1/6}$. In Figure 2 some examples of the images from the database are shown. It is important at this point to note that convolution kernels used by the CNES are not Gaussian. However, we will see that the approximate acquisition model of Section II yields good numerical results. In what follows, we will use the acquisition model (1) with a value $p = 1.3$. This value has been chosen as the value yielding the best numerical results (among values ranging from 1 to 2 by steps of 0.1) and it also corresponds to a rough approximation of the kernel used by the CNES.

B. Validity of the prediction scheme

First, we check the validity of Formula (8), (9) and (10) by plotting numerical values of features m_1 and m_2 as a function of the resolution.

In Figures 3 (d)-(f) (resp. (g)-(i)) graphs of $m_1(q,r,t)/r$ (resp. $m_2(q,r,t)/r^2$) as functions of r are presented when rt is kept constant (that is when using the naive normalization of Equation (11)) and when $r\sqrt{t^2+p^2}$ (with $p = 1.30$) is kept constant (see Equation (8)). The resolution r ranges from $0.50m$ to $4m$. For the image at resolution $0.50m$ (the highest available resolution), m_1 and m_2 are computed at scale 16 in the horizontal direction. It may be seen that using Equation (11) (that is forgetting the convolution step in the model of resolution change) does not yield a constant parameter set, especially when the resolution change is large. In contrast, using Equation (8) yields fairly constant values.

Next, we compare values of m_1 and m_2 computed on an image with resolution $3.175m$ to values of m_1 and m_2 computed on a image of the same scene with resolution $1m$ and then predicted for a resolution of $3.175m$. We perform this comparison for various scales. Figures 4 (a)-(c) (resp. (d)-(f)) show the values of m_1 (respectively m_2) at various scales

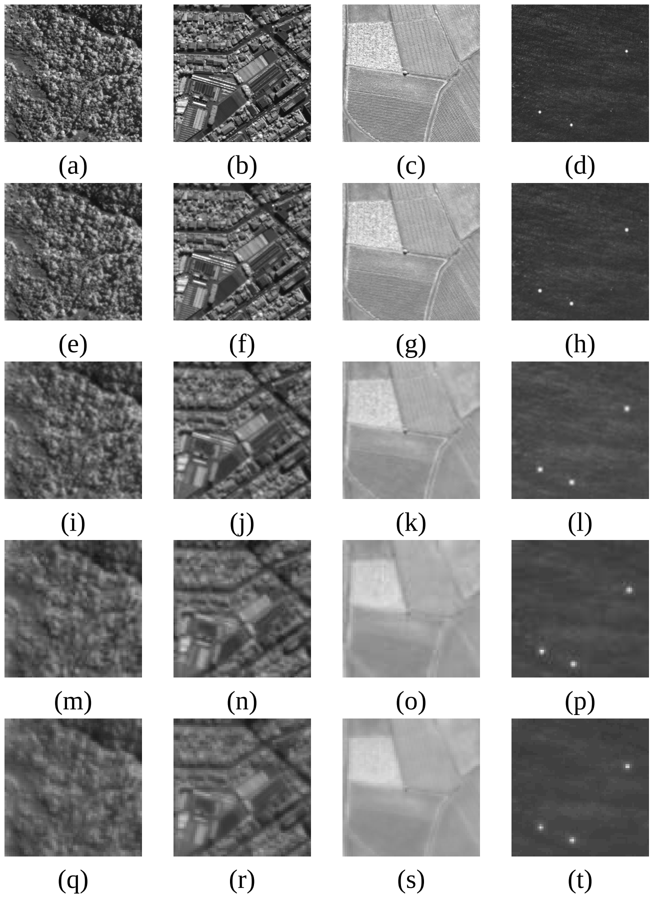

Fig. 2. Image samples from the database provided by the CNES: (a)-(d) Images at resolution $0.5m$; (e)-(h) Images at resolution $1.0m$; (i)-(l) Images at resolution $2.0m$; (m)-(p) Images at resolution $3.175m$; (q)-(t) Images at resolution $4.0m$; From left to right, classes of the images are: field, city, forest and sea.

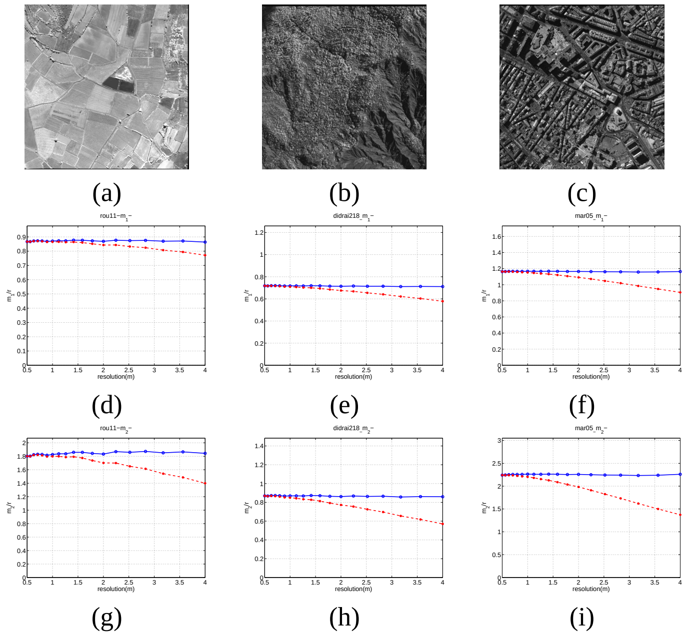

Fig. 3. **(a)-(c)** Three images (©CNES); **(d)-(f)** graphs of $m_1(q,r,t)/r$ (with $q=0$) as a function of r; **(g)-(i)** graphs of $m_2(q,r,t)/r^2$ (with $q=0$) as a function of r. On all these graphs, solid lines correspond to the case where $r\sqrt{t^2+p^2}$ is kept constant (with $p=1.3$), and dashed lines correspond to the case the case where rt is kept constant. One observes that using Equation (8) yields fairly constant values, whereas using Equation (11) does not.

(scale is on the horizontal axis) in solid blue line for three different scenes. On the same figure, m_1 (resp. m_2) predicted from a resolution of $1m$ for a resolution of $3.175m$ according to the scheme presented in Section IV-B are displayed by a solid red line. The two solid lines almost perfectly coincide. In dashed line, are plotted the values of m_1 (respectively m_2) predicted from a resolution of $1m$ for a resolution of $3.175m$ by the same scheme of Section IV-B, except that Equation (13) is replaced by $t'_i = r_1 t_i / r_2$. This corresponds to what we called the naive choice, neglecting convolutions in the resolution change. It can be seen that in this case, the guessed values of m_1 and m_2 are less accurate, especially for small scales. These experiments validate the scheme proposed in Section IV-B and suggests that it is necessary to take into account the convolution step in resolution changes to be able to compare features computed on images with different resolution. The next section investigates how the accuracy of the proposed scheme permits the classification of images at different resolutions.

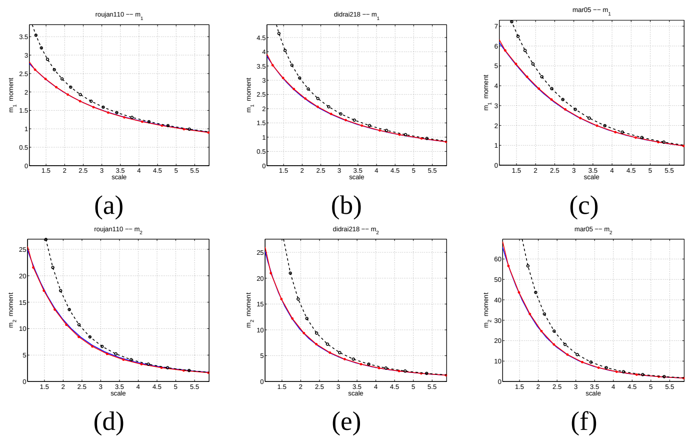

Fig. 4. Values of m_1 (**(a)-(c)**) and of m_2 (**(d)-(f)**) for various scales (scale corresponds to the horizontal axis). In solid red line are displayed the values computed directly on images with resolution $3.175m$ (the ground truth in this experiment). In solid blue line, are displayed the values first computed on the images with resolution $1m$ and then predicted using the scheme presented in Section IV-B. Both solid lines almost perfectly coincide, showing the accuracy of the scheme. Dash lines show the results obtained by using the scheme proposed in Section IV-B but replacing Equation (13) with $t'_i = r_1 t_i / r_2$ (the naive normalization). Observed and predicted values do not correspond anymore in this case.

C. Classification

a) Classified database: We have manually built a classified database based on the sequences of images provided

TABLE I

CLASSIFICATION RESULTS OBTAINED WITH WAVELET FEATURES EXTRACTED IN 4 DIRECTIONS AT 21 SCALES ($t = \{2^{i/6} | i = 0, 1, \ldots, 20\}$). THE LEARNING SET IS MADE OF IMAGES AT RESOLUTION $4m$.

Resolution	error ($p = 1.3$)	error ($p = 0$)
0.5m	0.00%	21.86%
1m	0.00%	19.95%
2m	0.00%	10.66%
3.175m	0.00%	1.91%

TABLE II

CLASSIFICATION RESULTS OBTAINED WITH WAVELET FEATURES EXTRACTED IN 4 DIRECTIONS AT 3 SCALES ($t = 1, 2, 4$). THE LEARNING SET IS MADE OF IMAGES AT RESOLUTION $4m$.

Resolution	error ($p = 1.3$)	error ($p = 0$)
0.5m	0.55%	26.50%
1m	0.00%	24.59%
2m	0.00%	12.84%
3.175m	0.27%	4.92%

by the CNES. This database contains 366 scenes observed on urban areas (Marseille and Toulouse), rural areas (Roujan), forests (Didrai) and the sea. For each scene, there are 5 different images corresponding to 5 different resolutions ($0.5m$, $1m$, $2m$, $3.175m$ and $4m$). The scenes are manually divided into 4 sets: city (199 scenes), fields (134 scenes), forests (23 scenes) and sea (10 scenes).

b) Experiment: The first experiment carried out on this database is classification. Images at the resolution of $4m$ are used as a learning set for training the classifier. The aim is to find the classes of the images at resolutions other than $4m$. Wavelet features (m_1 and m_2) are at first extracted from all the images by applying Gaussian derivatives at different scales in 4 directions (horizontal, vertical and diagonal). The features extracted from the images at a resolution of $4m$ over 21 scales ($t = \{2^{i/6}, i = 0, 1, \ldots, 20\}$) are used to train the classifier. Therefore the dimension of the feature space is $2 \times 4 \times 21 = 168$. The features extracted from the other resolutions are predicted at a resolution of $4m$ by using the scheme presented in Section IV-B. For comparison, we set the value p respectively equal to 1.3 (using the acquisition model) and 0.0 (the naive approach). We then classify the images at resolutions other than $4m$ with the predicted features.

The classifier we used is simply the nearest neighbor classification algorithm. For a given image A, the classifier search for its nearest neighbor B in the training set and affect to A the class of B. As a distance between features, we use the Euclidean distance, after normalizing each coordinate by its variance.

c) Results: The classification results are shown in Tab. I. It can be observed that with the naive approach, the classification errors increase rapidly when the resolution gets away from $4m$. This shows numerically that the naive approach ($p = 0$) is not a good choice for classification purpose. On the contrary, when the acquisition model is taken into consideration (i.e. $p = 1.3$), there is no error. This is due to the fact that the prediction scheme is very accurate, as we have shown in Section V-B. Errors are small enough not to switch from one class to another when changing the resolution.

d) Influence of the number of features: The classification results presented in Table I are obtained from features in a space with relatively large dimension (168 values for each image). We therefore study the effect of a dimension reduction. In Table II are shown the classification results obtained when performing the same experiment as in Table I, using the wavelet features (m_1 and m_2) at only 3 scales ($t = 1, 2, 4$). In this case the dimension of the feature space is $2 \times 4 \times 3 = 24$ and it can be observed that the errors remain similar.

TABLE III

CLASSIFICATION RESULTS OBTAINED WITH HARALICK FEATURES. THE DISTANCE PARAMETER FOR CALCULATING CO-OCCURRENCE MATRICES VARIES ACCORDING TO THE RESOLUTION OF IMAGE. THE LEARNING SET IS MADE OF IMAGES AT RESOLUTION $4m$.

Resolution	distance	error
0.5m	24	31.9%
1m	12	22.4%
2m	6	13.6%
3.175m	4	10.1%

e) Comparison with other features: In order to further investigate the effect of resolution changes on classification tasks, we perform an experiment using Haralick features. Haralick [29] has proposed features based on the statistics of co-occurrence matrices of images. These features are proved to be very efficient for indexing textures. Co-occurrence matrices are defined as the empirical joint distribution of the gray values of pixels in some direction θ and at some distance d. The considered directions are horizontal, vertical and two diagonal directions. The distance between the pixel pairs can be considered as a scale parameter. For images at different resolutions, it is therefore natural to compute co-occurrence matrices with different distances. In our experiment, we set $d = 3, 4, 6, 12, 24$ respectively for images at resolutions $4m$, $3.175m$, $2m$, $1m$ and $0.5m$. These values ensure that $d \times r$ is a constant. The Haralick features are composed of 13 statistical values calculated from each matrix and the mean and standard deviation values through the four directions. Therefore the total feature dimension is $(4 + 2) \times 13 = 78$.

Figure III shows the classification results obtained with Haralick features. Our purpose here is not to compare directly these results with the results obtained in the previous section. Indeed, results obtained with wavelet features are better, but we did not take full advantages of co-occurrence matrices since only one scale is used for each image. The interesting point is to notice how fast the classification results decrease with the change of resolution, therefore showing the inability of Haralick features to handle such changes. Observe that the approach taken here is similar to the naive choice of previous sections (approximating a resolution change through a zoom). Due to the non-linear nature of co-occurrence matrices, the approach proposed in the case of wavelet features is not adaptable to Haralick features.

TABLE IV

MISMATCHING PERCENTAGES WHEN USING WAVELET FEATURES EXTRACTED AT 21 SCALES WITH 4 ORIENTATIONS.

resolution	0.5	1.0	2.0	3.175
p=1.3	4.1	0.27	0	1.64
p=0	81.97	79.51	65.57	34.97

TABLE V

MISMATCHING PERCENTAGES WHEN USING WAVELET FEATURES EXTRACTED AT 3 SCALES WITH 4 ORIENTATIONS

resolution	0.5	1.0	2.0	3.175
p=1.3	11.2	4.64	1.09	9.29
p=0	95.90	96.45	92.62	62.02

D. Image Matching

In this subsection, we carry out a more difficult experiment than in the previous subsections. For each image at a resolution of $4m$, we want to find the exact same scene from the images at other resolutions with the help of wavelet features. The features are extracted and predicted as presented in Section IV-B. For an image at a resolution different from $4m$, we search its nearest neighbor in the feature space among the set of images at $4m$. If the two images represent the same scene, it is a correct match, otherwise it is an error. This is the same classification task as before, except that we consider each scene to be a class in itself.

In Table IV are displayed the matching results when using features over 21 scales ($t_i = 2^{i/6}$, $i = 0, 1, \ldots, 20$) and 4 orientations. In Figure V are displayed the matching results when using only 3 scales ($t_i = 2^i$, $i = 0, 1, 2$).

It can be observed that

- The errors increase considerably when compared to the classification results of the previous subsection, especially when $p = 0.0$. This is due to the fact that in the image database, there are many scenes of the same class which are very similar one to another. Therefore the points representing these images in the feature space are close one to another. As a consequence, a small error in the prediction causes an error in the image matching, in contrast with the classification case of Section V-C.
- The small errors in the case $p = 1.3$ confirm the accuracy of the scheme.

VI. CONCLUSIONS AND PERSPECTIVES

In this paper, we have proposed a scheme for comparing wavelet features from images taken at different resolutions.

The acquisition of images is modeled by a convolution followed by a sampling. The scheme to compare wavelet features is based on this model and the semi-group property of the Gaussian kernel. We first checked experimentally the validity of this scheme and showed that the numerical accuracy is significantly improved compared to a naive approach where resolution change is simply modeled by a zoom. This approach is then applied for the classification of satellite images at several resolutions simulated by the CNES. Our approach improves significantly the accuracy of the classification. This fact is confirmed trough an image matching experiment.

The method presented in Section IV-B to compare wavelet features between images with different resolution is quite general. We applied it to image classification, but other tasks could benefit from this approach. For instance, the scale invariance of wavelet transformations has been applied to the fusion of aerial images having different resolutions [30][31][32]. None of these works takes into account the influence of the optics and captors on the change of resolution. We believe that the approach presented in Section IV could improve the precision of such fusions of images.

Acknowledgements: We thank Mihai Datcu, Alain Giros and Henri Maître for their advices and comments.

APPENDIX

In this appendix, we detail the approximation made in Equation (5) and compute the error functions of the approximation made in Equation (6).

Recall that $w_{q,r,t}$ are the wavelet (Gaussian derivative) coefficients extracted from f_r at scale t and in direction q, where f_r is the digital image at resolution r obtained from the continuous scene f. For clarity, we only consider the $1D$ case. Recall Formula (5):

$$\begin{aligned} w_{q,r,t} &= \Delta_q \tilde{k}_t \tilde{*} \Pi_r(k_{rp} * f) \\ &= \tilde{k}_t \tilde{*} \Delta_q \Pi_r(k_{rp} * f). \end{aligned}$$

In the $1D$ case, we have

$$w_{r,t} = \tilde{k}_t \tilde{*} \Delta_x \Pi_r(k_{rp} * f).$$

Writing $g(x) = (k_{rp} * f)(x)$, we have

$$\begin{aligned} w_{r,t}(x) &= \tilde{k}_t \tilde{*} \Delta_x \Pi_r(g(x)) \\ &= \tilde{k}_t \tilde{*} (\Pi_r(g(x + r) - g(x))), \end{aligned}$$

and since $g \in C^1$, we have

$$g(x + r) = g(x) + rg'(x) + o(r).$$

Therefore

$$\begin{aligned} w_{r,t} &\approx \tilde{k}_t \tilde{*} \Pi_r(g(x) + rg'(x) - g(x)) \\ &= \tilde{k}_t \tilde{*} \Pi_r(rg'(x)) \\ &\approx r\tilde{k}_t \tilde{*} \Pi_r(k_{rp} * f'(x)). \end{aligned}$$

This is the approximation made in Equation (5). Next, we compute the error energy of the approximation made in Equation (6). For simplicity, we consider the resolution $r = 1$. We want to show that the energy of the error is small.

$$\begin{aligned} E &= \sum |\Delta_x \tilde{k}_t * \Pi_1(g) - \Pi_1(k_t * g')|^2 \\ &= \int |FT\left\{\Delta_x \tilde{k}_t * \Pi_1(g) - \Pi_1(k_t * g')\right\}|^2 d\omega \end{aligned}$$

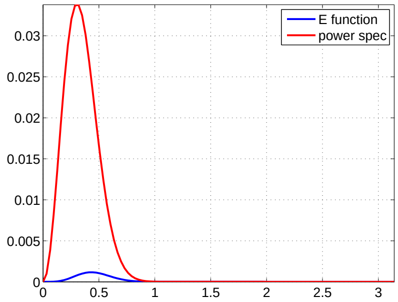

Fig. 5. Error function (E) and power spectrum of wavelet coefficients $w_{r,t}$ in the frequency domain.

where $FT(f)$ is the Fourier transform of f. With the approximation $k_t \approx \Pi_r(k_{rt})$, we have

$$\begin{aligned} E &\approx \int |FT\{\Delta_x \Pi_1(k_t * g) - \Pi_1(k_t * g')\}|^2 d\omega \\ &= \int |FT\{\Pi_1(k_t * g(x+1) - k_t * g(x)) - \Pi_1(k_t * g')\}|^2 d\omega \\ &= \int |FT\{\Pi_1(k_t * g(x+1) - k_t * g(x) - k_t * g')\}|^2 d\omega \end{aligned}$$

We suppose that the image is not aliased, (i.e. $k_t * g$ is band limited), therefore

$$\begin{aligned} E &\approx 2\int_0^\pi |FT\{k_t * g(x+1) - k_t * g(x) - k_t * g'\}|^2 d\omega \\ &= 2\int_0^\pi |e^{j\omega} - 1 - j\omega|^2 |FT\{k_t * g\}|^2 d\omega \\ &= 2\int_0^\pi (2(1-\cos\omega - w\sin\omega) + \omega^2)\, |FT\{k_t * g\}|^2 d\omega \\ &\approx 2\int_0^\pi \left(2(-\frac{\omega^2}{2} + \frac{\omega^4}{8}) + \omega^2\right) |FT\{k_t * g\}|^2 d\omega \\ &\approx \int_0^\pi \frac{\omega^4}{2} |FT\{k_t * k_p * f\}|^2 d\omega \\ &= \int_0^\pi \frac{\omega^4}{2} |FT\{k_{\sqrt{p^2+t^2}}\}|^2 |FT\{f\}|^2 d\omega. \end{aligned}$$

Recall that $t \geq 1$ and $p = 1.3$ in all our numerical experiments. Since the power spectrum of the image f is generally decreasing, and $\frac{\omega^4}{2}$ is increasing, the worst case (which yields the largest error) is therefore $|FT\{f\}|^2 = 1$ for all ω, where we have

$$E \approx \int_0^\pi \frac{\omega^4}{2} |FT\{k_{\sqrt{1^2+1.3^2}}\}|^2 d\omega$$

and

$$\frac{E}{\sum |w_{r,t}|^2} \approx 0.035.$$

Figure 5 shows a plot of E and the power spectrum of wavelet coefficients $w_{r,t}$ in the frequency domain for the case where $|FT\{f\}|^2 = 1$. In the worst case, the approximation made in Equation (6) yields an energy error of 3.5% when compared to the energy of the original wavelet coefficients.

References

[1] D.G. Lowe, “Distinctive image features from scale-invariant keypoints,” *International Journal of Computer Vision*, vol. 60, no. 2, pp. 91–110, 2004.

[2] Fernand S. Cohen Zhigang Fan and M. A. Patel, “Classification of rotated and scaled textured images using gaussian markov random field models,” *IEEE PAMI*, vol. 13, no. 2, pp. 192–202, February 1991.

[3] Jianguo Zhang and Tieniu Tan, “Affine invariant texture signatures,” in *ICIP 2001*, Oct. 2001, vol. 2, pp. 618–621.

[4] C. M. Pun and M. C. Lee, “Log-polar wavelet energy signatures for rotation and scale invariant texture classification,” *IEEE PAMI*, vol. 25, no. 5, pp. 590–603, 2003.

[5] J. Zhang and T. Tan, “A brief review of invariant texture analysis methods,” *Pattern Recognition*, vol. 35, pp. 735–747, 2002.

[6] B. Luo, J-F. Aujol, Y. Gousseau, S. Ladjal, and H. Maître, “Characteristic scale in satellite images,” in *ICASSP 2006*, May 2006, vol. 2, pp. 809–812.

[7] B. Luo, J-F. Aujol, Y. Gousseau, S. Ladjal, and H. Maître, “Resolution independant characteristic scale dedicated to satellite images,” *IEEE Trans. on Image Processing*, vol. 16, no. 10, pp. 2503–2514, 2007.

[8] Jan Flusser and Tomas Suk, “Degraded image analysis: An invariant approach,” *IEEE PAMI*, vol. 20, no. 6, June 1998.

[9] J. van de Weijer and C. Schmid, “Blur robust and color constant image description,” in *International Conference on Image Processing*, 2006.

[10] A. Lorette, X. Descombes, and J. Zerubia, “Texture analysis through a markovian modelling and fuzzy classification: Application to urban area extraction from satellite images,” *International Journal of Computer Vision*, vol. 36, no. 3, pp. 221–236, 2000.

[11] G. Rellier, X. Descombes, F. Falzon, and J. Zerubia, “Texture feature analysis using a gauss-markov model in hyperspectral image classification,” *IEEE Transactions on Geoscience and Remote Sensing*, vol. 42, no. 7, pp. 1543–1551, 2004.

[12] M. Datcu, K. Seidel, and M. Walessa, “Spatial information retrieval from remote-sensing images. ii. information theoretical perspective,” *IEEE Trans. Geoscience and Remote Sensing*, vol. 36, no. 5, pp. 1431–1445, 1998.

[13] K. Chen and R. Blong, “Identifying the characteristic scale of scene variation in fine spatial resolution imagery with wavelet transform-based sub-image statistics,” *International Journal of Remote Sensing*, vol. 24, no. 9, pp. 1983–1989, 2003.

[14] T. Gevers and H. Stokman, “Robust photometric invariant region detection in multispectral images,” *IJCV*, vol. 53, pp. 135–151, July 2003.

[15] D. Van Dyck G. Van de Wouwer, G. Scheunders, “Statistical texture characterization from discrete wavelet representations,” *IEEE Trans. on Image Processing*, vol. 8, no. 4, pp. 592–598, 1999.

[16] Minh N. Do and Martin Vetterli, “Wavelet-based texture retrieval using generalized gaussian density and kullback-leibler distance,” *IEEE Transactions on Image Processing*, vol. 11, no. 2, pp. 146–158, February 2002.

[17] J-F. Aujol, G. Aubert, and L. Blanc-Féraud, “Wavelet-based level set evolution for classification of textured images,” *IEEE Transactions on Image Processing*, vol. 12, no. 12, pp. 1634–1641, 2003.

[18] M. Unser, “Texture classification and segmentation using wavelet frames,” *IEEE Transactions on Image Processing*, vol. 4, no. 11, pp. 1549–1560, November 1995.

[19] H. Choi and R.G. Baraniuk, “Multiscale image segmentation using wavelet-domain hidden markov models,” *IEEE Transactions on Image Processing*, vol. 10, no. 9, pp. 1309–1321, September 2001.

[20] G. Van de Wouwer, P. Scheunders, and D. Van Dyck, “Statistical texture characterisation from discrete wavelet representation,” *IEEE IP*, vol. 8, no. 4, pp. 592–598, 1999.

[21] J. Liu and P. Moulin, “Information-theoretic analysis of interscale and intrascale dependencies between image wavelet coefficients,” *IEEE Transactions on Image Processing*, vol. 10, no. 11, pp. 1647–1658, November 2001.

[22] J.L. Chen and A. Kundu, “Rotation and gray scale transform invariant texture identification using wavelet decomposition and hidden markov model,” *IEEE Transactions on Pattern Analysis and Machine Intelligence*, vol. 16, no. 2, pp. 208–214, February 1994.

[23] Soe Win Myint, Nina S.-N. Lam, and John M. Tyler, “Wavelets for urban spatial feature discrimination: Comparisons with fractal, spatial autocorrelation, and spatial co-occurence approaches,” *Photogrammetric Engineering and Remote Sensing*, vol. 70, pp. 803–812, July 2004.

[24] B. Luo, J-F. Aujol, Y. Gousseau, and S. Ladjal, "Interpolation of wavelet features for satellite images with different resolutions," in *IGARSS*, Denver USA, 2006.

[25] D.F. Ellliott, L.L. Hung, E. Leong, and D.L Webb, "Accuracy of gaussian approximation for simulating eo sensor response," in *Conference Record of the Thirtieth Asilomar Conference on Signals, Systems and Computers 1996*, 1996, pp. 868–872.

[26] B. Zhang, J. Zerubia, and J.C. Olivo-Marin, "Gaussian approximations of fluorescence microscope point-spread function models," *Applied Optics*, vol. 46, no. 10, pp. 1819–1829, avril 2007.

[27] Stephane G. Mallat, "A theory for multiresolution signal decomposition: The wavelet representation," *IEEE PAMI*, vol. 11, no. 7, pp. 674–693, July 1989.

[28] S.G. Mallat, *A Wavelet Tour of Signal Processing*, Academic Press, 1998.

[29] R.M. Haralick, K. Shanmugam, and I. Dinstein, "Textural features for image classification," *IEEE Transactions on Systems Man and Cybernetics*, vol. SMC-3(6), 1973.

[30] Ranchin Thierry, "Remote sensing and image fusion methods: A comparison," *ICASSP 2006 Proceedings. 2006 IEEE International Conference on Acoustics, Speech and Signal Processing, 2006.*, vol. 5, May 2006.

[31] Gang Hong and Yun Zhang, "High resolution image fusion based on wavelet and ihs transformations," *2nd GRSS/ISPRS Joint Workshop on Remote Sensing and Data Fusion over Urban Areas, 2003*, pp. 99–104, May 2003.

[32] Núnez J., Otazu X., Fors O., Prades A., Pala V., and Arbiol R., "Multiresolution-based image fusion with additive wavelet decomposition," *IEEE Transactions on Geoscience and Remote Sensing*, May 1999.